Open Access Book Chapter

Published version

Chapter title	Charge Carrier Dynamics in Organometal Halide Perovskite Probed by Time-Resolved Electrical Measurements
Title in English	
Author(s)	Carlito S. Ponseca Jr.
DOI	10.5772/61631
Copyright holder	**The Authors**
License	Creative Commons Attribution License (http://creativecommons.org/licenses/by/3.0)
Language	English

Original publication

Book title	Perovskite Materials - Synthesis, Characterisation, Properties, and Applications
Title in English	
Publisher	**Intech**
Publication date	2016
ISBN	**9789535122456**
DOI	
Editor(s)	Likun Pan and Guang Zhu

ERC Grant information

Project title	EC | VISCHEM
Project acronym	Vischem
Grant number	226136
ERC principal investigator	Villy Sundström

OAPEN Foundation received funding from the European Research Council (ERC)
under the European Union's Horizon 2020 research and innovation programme (grant agreement No 683680).

Chapter 11

Charge Carrier Dynamics in Organometal Halide Perovskite Probed by Time-Resolved Electrical Measurements

Carlito S. Ponseca Jr.

Additional information is available at the end of the chapter

http://dx.doi.org/10.5772/61631

Abstract

This chapter presents the fate of the charge carriers from the moment of its photogeneration in the perovskite to injection and transport into electrodes. Time-resolved electrical measurement techniques, terahertz (THz) spectroscopy and microwave (MW) conductivity, are primarily used to deconvolute ultrafast processes and to directly access behavior of charged species from the ps to μs timescales. Transient absorption and photoluminescence spectroscopy were also utilized to gain insight on carrier population dynamics and radiatively recombining charges. Photogenerated charged species were converted into highly mobile charges (μ_e = 12.5 $cm^2V^{-1}s^{-1}$ and μ_h = 7.5 $cm^2V^{-1}s^{-1}$) almost instantaneously (< 0.2 ps), while the remaining loosely bounded excitons dissociate into mobile charges after 2-3 ps. This high mobility is maintained for at least 1 ns as obtained by THz spectroscopy, while its lifetime is at least few tens of μs as measured by the MW conductivity technique. Lowering the temperature increases carrier mobilities with $T^{-1.6}$.Dependence and a 75 meV barrier energy is required for temperature-activated recombination. Finally, injection of hole from $MAPbI_3$ to Spiro-OMeTAD was found to be ultrafast and the state and population of dark holes dictate its recombination.

Keywords: THz spectroscopy, Time-resolved Microwave Conductivity (TRMC), photoconductivity, mobility

1. Introduction

The qualities of highly efficient solar cell material are its ability to absorb light with the widest spectral range possible, high light-to-charge conversion ratio, and transport of these charges to electrodes with least losses. This seems to be the case in organometal halide perovskite (OMHP)-based solar cell as its overall power conversion efficiencies (PCEs) have risen from a

meagre 4% [1] to 20.1% [2] to date. Such increase has not been seen in any other solar cell technology since the conception of light harvesting. In fact, the PCE of dye-sensitized solar cell, where the OMHP was first used as a dye substitute, remained modest [2]. In recent years, spectroscopic studies on these materials have started to trickle the much-needed fundamental investigations. Most of its well-known characteristics include electron-hole diffusion lengths longer than one micrometer [3], high mobility, and very slow recombination [4]. Despite this, there is a long list of unexplained early timescale processes, which is fundamental to understating its solar cell function. For instance, details whether molecular excitons or to highly mobile charges are the initial photoproduct and how is this related to the exceptionally long diffusion lengths, remains unanswered. It is also unclear to what extent generation and recombination of mobile charges are affected by temperature. The use of metal oxide electrodes such as TiO_2 and Al_2O_3, as electron acceptor and isolating nanoparticles (NP), respectively, and their role on its electronic properties has not yet been understood. Many groups have also recently attempted to use organic electrodes, e.g., PCBM and Spiro-OMeTAD and were able to get decent PCE. Questions on its charge transfer mechanism, timescale, and details of injection are yet to yield convincing answers.

In this chapter, an ensemble of spectroscopic techniques, primarily time-resolved terahertz spectroscopy (TRTS) and time-resolved microwave conductivity (TRMC) complemented by photoluminescence and transient absorption, was used to monitor the creation of charged species induced by photoexcitation at the sub-ps timescale and probe its fate up to a hundred of microsecond. Both techniques have been used in an assortment of solar cell technologies including organic [5,6], dye-[7], and quantum dot- sensitized [8], and inorganic [9] systems. Neat methylammonium lead iodide ($MAPbI_3$) was used to study the intrinsic transport properties of perovskite material both at room and low temperatures. To determine how electron accepting metal and the role of NP in general, $MAPbI_3$ were introduced to TiO_2 and Al_2O_3, respectively. Charge transfer mechanism and the corresponding recombination dynamics when attached to organic electrodes, PCBM and Spiro-OMeTAD were also explored. Note that detailed discussion of different material contacts, their heterogeneity, and their morphologies' influence on charge carrier dynamics are presented in Ref. [10].

On light excitation, changes in conductivity from ground state (σ) to photo-induced or transient state ($\Delta\sigma$) are measured in the solar cell material. This conductivity when normalized with charge density yields mobility (μ) per charge carrier. This photoconductivity is measured at high frequencies, i.e., at the THz regime (0.1–1.5 THz) and at the GHz regime (12 GHz). As such, these high-frequency waves are propagating through free space and are able to interrogate the sample without any electrodes. The TRTS and TRMC signal size can be expressed as product of two quantities, quantum yield, and electron and hole mobilities ($\mu_e + \mu_h$). This product is calculated according to:

$$\Delta\sigma = \varphi \times \left(\mu_e + \mu_h\right) = \frac{\Delta\sigma L}{eI_0 F_A}$$

where $\Delta\sigma$ is the measured change in photoconductivity, L is the thickness, e is the elementary charge, I_0 is the number of photons per unit area per pulse, and F_A is the fraction of absorbed

http://dx.doi.org/10.5772/61631

light. A rise in the photoconductivity kinetics signals either creation of charged species, since only these photoproducts can induce changes in conductivity or an increase in mobility. On the other hand, decay in the kinetics means disappearance of these species, through recombination, injection to lower mobility acceptor molecules, and/or decrease in mobility.

Section 2 of this chapter presents the early timescale generation mechanism of charge carrier in neat perovskite in order to understand the intrinsic property of this material. It also discusses the influence of NPs, TiO_2, and Al_2O_3 on the mobility of the photo-induced carriers. In Section 3, a discussion on the fate of the charges when temperature is lowered will be presented and relate these results to the origin of the very long recombination time. Lastly, in Section 4, the mechanism of electron and hole injection to organic electrodes, PCBM and Spiro-OMeTAD, is reported and the role of dark carriers in the recombination dynamics is discussed.

2. Probing the charge carrier dynamics of intrinsic $MAPbI3_3$

The early time THz photoconductivity kinetics of neat $MAPbI_3$, $MAPbI_3/Al_2O_3$ and $MAPbI_3/TiO_2$ is shown in Fig. 1a. For both $MAPbI_3$ and $MAPbI_3/Al_2O_3$, a two-step increase is observed. An instrument-limited rise with amplitude of about 70% is followed by 2-3 ps increase of about 30%. Tightly bound molecular excitons are, by definition, neutrally charged and hence cannot affect the conductivity of the material. This means that even if these excitons are generated, their contribution to the THz signal is nil. Therefore, the sub-ps increase in the photoconductivity kinetics comes from generation of charged species. It was reported that the binding energy of exciton in these materials may vary between 4 meV [11] to 50 meV [12]. The heterogeneity of the binding energy in a material could cause photogenerated species to dissociate at different rates. As such, the slower rise in the kinetics could be due to separation of loosely bounded charge pair becoming independent charges. Initially, charges bounded by Coulombic force require an energy that could separate them; in this case it seems enough that thermal energy, kT, dissociates them and only takes few ps, 2-3 ps rise in the THz kinetics of neat $MAPbI_3$ and $MAPbI_3/Al_2O_3$. Unlike the previous two samples, for $MAPbI_3/TiO_2$ the THz transient rises faster and reaches the maximum signal with a single-step instrument-limited rise time. It was reported before that light absorbers attached to metal oxide of high electron affinity, ultrafast electron injection can be expected. For example, RuN3 dye attached to TiO_2 [7] and in CdSe quantum dot attached to ZnO [8] shows ultrafast injection. Therefore, the ultrafast limited rise in THz kinetics of $MAPbI_3/TiO_2$ is due to sub-ps injection of electrons from the OMHP to TiO_2. Favorable alignment of energy band levels between the perovskite and metal oxide aides the separation of any remaining loosely bound electron–hole pair favoring ultrafast injection. This is the reason why there is no second-step rise seen in the THz kinetics. Shown in Fig. 1b is the THz kinetics per photon absorbed per pulse. It shows that the mobility of $MAPbI_3/TiO_2$ is 7.5 $cm^2V^{-1}s^{-1}$, about 3-4 smaller lower than the mobility in neat $MAPbI_3$ and the $MAPbI_3/Al_2O_3$, which is 20 $cm^2V^{-1}s^{-1}$. The difference in the mobility also supports the proposal that electron injection occurs in $MAPbI_3/TiO_2$. From the total mobility of neat $MAPbI_3$, electrons disappear due to their injection to TiO_2. Because of this, only the holes left in the perovskite are seen by the instrument, resulting in lower mobility.

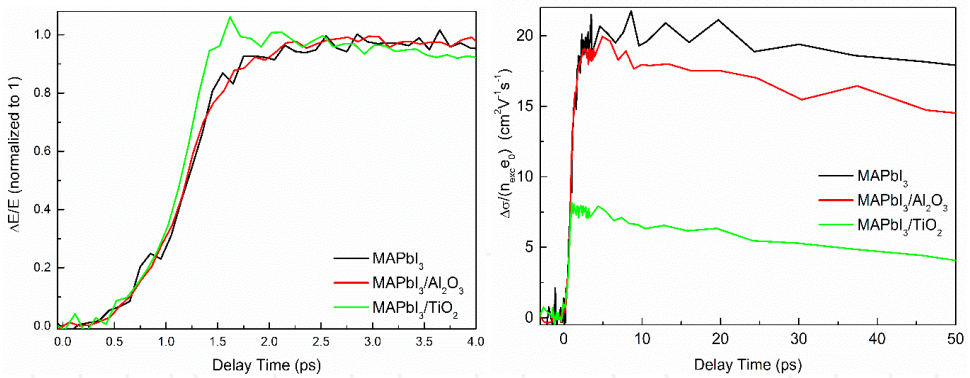

Figure 1. THz photoconductivity kinetics of neat $MAPbI_3$, $MAPbI_3/Al_2O_3$, and $MAPbI_3/TiO_2$. a. Normalized to 1 (λ_{pump} = 400 nm, I_{exc} = 1.7 x 10^{13} ph/cm^2 per pulse), b. Normalized with $n_{exc}e$. (Reprinted with permission from [57], Copyright 2014, American Chemical Society)

To further confirm electron injection, optical transient absorption (TA) was used to probe the arrival of electrons to TiO_2 after photoexciting the perovskite layer. The normalized TA kinetics of neat $MAPbI_3$ and $MAPbI_3/Al_2O_3$ are shown in Fig. 2a. It has a response-limited rise (negative), and then an approximately 2 ps of further decrease, very similar to the two-component increase in THz photoconductivity kinetics, showing that indeed there are charges that are not created right away. The negative signal, probed 970 nm is a part of the spectral region where there is no ground state absorption, and therefore indicative of stimulated emission. This is consistent with the ground state photoluminescence (PL) emission spectra (Fig. 2b) showing intense emission from these two samples. On the other hand, an ultrafast rise with only one component with positive sign, which means absorption, is obtained in the kinetics of $MAPbI_3/TiO_2$. This is in agreement with the timescale of arrival of electrons in TiO_2 [10,13] and very similar to the THz kinetics (Fig. 1a). Despite the fact that there is still some emission, the strong quenching of photoluminescence in $MAPbI_3/TiO_2$ is an additional proof that there is injection of electrons. From the SEM image of the three samples (Fig. 3), $MAPbI_3/TiO_2$ shows no indication of domains of $MAPbI_3$ bigger than 500 nm, meaning that the mesoporous network of $MAPbI_3$ is formed within TiO_2 NPs analogous to that reported in Ref. [13]. Despite this, reduced domains of $MAPbI_3$ may still be formed brought about by voids due TiO_2 NPs. However, this could be small, as shown by the strong quenching of emission and the fast rise in THz photoconductivity kinetics.

As shown in Fig. 1b, the first 40 ps of the THz kinectics for the three samples manifests a slow decay. It is usually assumed that at the earliest timescale, quantum yield is 1. At later timescale, the THz photoconductivity becomes a product of charge concentration and mobility since photogenerated charges are either starting to recombine or lose their mobility. In such case, it is not clear to conclude, based only on the photoconducivity kinetics, if the decay is related to depopulation of charges or lowering mobility with time or both. Transient absorption is the appropriate technique to measure the charge population as a function of time. Shown in Fig.

http://dx.doi.org/10.5772/61631

4a are kinetic traces of neat $MAPbI_3$, obtained through TA and TRTS at similar pump levels (~10^{13} ph/cm^2 per pulse). Within the signal-to-noise, the decay of the two plots is identical. This implies that the decay in the THz kinetics should be coming from the depopulation of charge carriers since the TA kinetics has the same decay. Consequently, this means that mobility of charge carrier remains the same at least up to 1 ns, otherwise a faster decay in the THz kinetics would be observed. To determine the reason for the depopulation of charges, the excitation density dependence of THz kinetics was obtained. At the lowest pump excitation (Fig. 4b, 2.0 × 10^{12} ph/cm^2 per pulse), the kinetics remained flat until 200 ps, where mobility obtained is 25 cm^{2}V^{-1}s^{-1}. These highly mobile charges measured in THz for OMHP material are within the same order reported by Wehrenfennig, et al. [4]. At highest intensity, the decay is fastest and mobility lowest. These are strong indications that the decay is due to non-geminate recombination of charges, similar to those reported in bulk heterojunction solar cell [5,6].

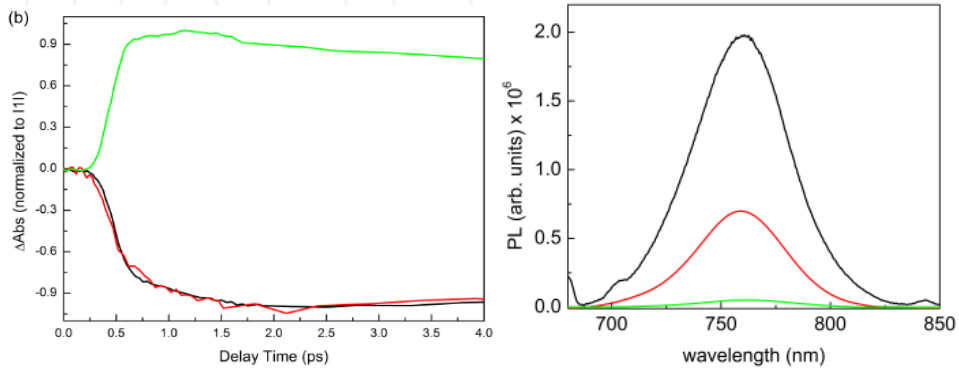

Figure 2. a. Transient absorption kinetics (λ_{pump} = 603 nm, λ_{probe} = 970 nm, I_{exc} = 6.0 x 10^{14} ph/cm^2 per pulse) b. Photoluminescence spectra (λ_{pump} = 550 nm) of the three samples. (Reprinted with permission from [57], Copyright 2014, American Chemical Society)

With the very high mobility of charges, it is interesting to know the nature of charge carrier transport. The THz photoconductivity spectra is a very useful tool in determining whether charges are behaving like free electron gas or in a confined, hopping-like manner. For this reason, the THz spectra of the three samples were measured after photoexcitation, i.e., at 10 ps as shown in Fig. 5. Within the signal-to-noise, the amplitude and also the shape of THz photoconductivity spectra are identical for neat $MAPbI_3$ and $MAPbI_3/Al_2O_3$. However, the spectral shape of $MAPbI_3/TiO_2$ is qualitatively different as well as its signal size is lower by four times. The real part of the conductivity is positive while the imaginary part is negative. From these observations several conclusions can be drawn. First, the THz photoconductivity kinetics as well as the spectra (Figs. 1a and 1b), and TA kinetics of neat $MAPbI_3$ and $MAPbI_3/Al_2O_3$ (Fig. 2a) show that Al_2O_3 NPs do not change the dynamical properties and mobility of charge carriers in perovskite, at least on the timescale probed by the THz measurements (1 ns). Secondly, the favorable band energy alignment between TiO_2 NPs and perovskite causes ultrafast injection, as shown in the reduction of signal size in the THz photoconductivity

kinetics (Fig.1b) and spectra (Fig. 5). As consequence of injection to TiO_2, the mobility of electrons becomes the mobility of TiO_2 (0.1 $cm^2V^{-1}s^{-1}$), which leads to unbalanced transport of charges. Third, sign of real and imaginary parts of conductivity is a signature of confined motion of charges [6], which is rather counterintuitive considering the very high mobility obtained here. One could hypothesize that at the spatial vicinity of photogeneration, maybe tens of nm, the morphology of the material is very much favorable for fast motion of the charges. However, at larger spatial scale, charges may start encountering scattering centers, e.g., traps, which can make its motion more restricted. The THz spectra (Fig. 5), which is normalized, decay due to non-geminate recombination as well as with excitation density, at several delay times (100–950 ps), are identical, supporting the interpretation that mobility is constant for 1 ns but with confined mode of transport.

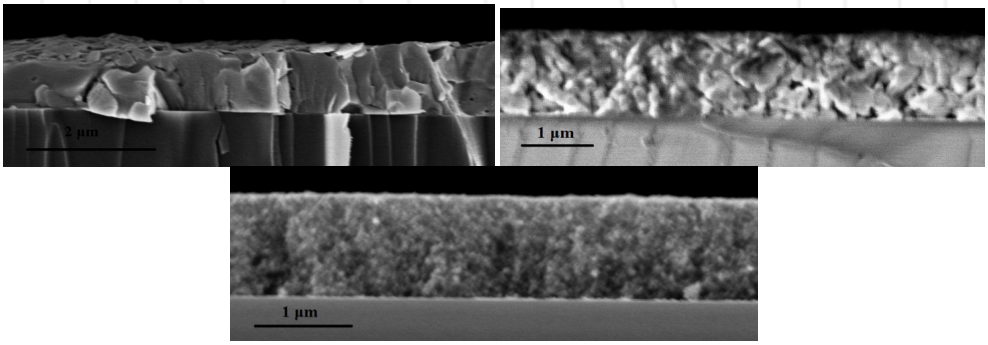

Figure 3. Scanning electron microscope image of a. neat $MAPbI_3$, b. $MAPbI_3/Al_2O_3$ and c. $MAPbI_3/TiO_2$. (Reprinted with permission from [57], Copyright 2014, American Chemical Society)

Differences in the mobilities of electrons and holes, typical with bulk heterojunction organic solar cells, which are sometimes several orders of magnitude, lowers the overall PCE due to built-in electric field brought about by space-charge-limited photocurrents [14]. This is because one of the charges has already reached the electrode while the other is still traversing the active layer of the solar cell. Therefore, it is important to assess not only the total mobility of the materials but to estimate both mobility of electrons and holes. Admittedly, THz measurement on one material alone would not provide this information, but rather by comparing it with known electron or hole mobilities this could be answered. The reported intrinsic electron mobility of porous TiO_2 films as measured by THz is <<1 $cm^2V^{-1}s^{-1}$ [15]. As shown in Fig. 1b, the mobility obtained for $MAPbI_3/TiO_2$ is 7.5 $cm^2V^{-1}s^{-1}$. From the discussion above, it was established that there is an ultrafast injection of electrons from perovskite to TiO_2, meaning that it should only be the mobility of holes that are left in the perovskite material that is seen by the instrument. As a consequence, the measured THz mobility of ~20 $cm^2V^{-1}s^{-1}$ for $MAPbI_3$ and $MAPbI_3/Al_2O_3$, where both electrons and holes are in the perovskite material and therefore contributing to the THz signal, 12.5 $cm^2V^{-1}s^{-1}$ should be coming from electrons since 7.5 $cm^2V^{-1}s^{-1}$ is from the holes. The resulting ratio of electron and hole mobilities in the perovskite is therefore about two, in agreement with the recent theoretical calculations of the relative effective masses of electrons and holes [16]. This also justifies the balanced long

http://dx.doi.org/10.5772/61631

diffusion lengths reported by the group of Stranks et al. [3, 17, 45]. The almost balanced electron and hole mobility is a unique key information rationalizing high PCE in OMHP-only or OMHP/Al_2O_3 solar cells.

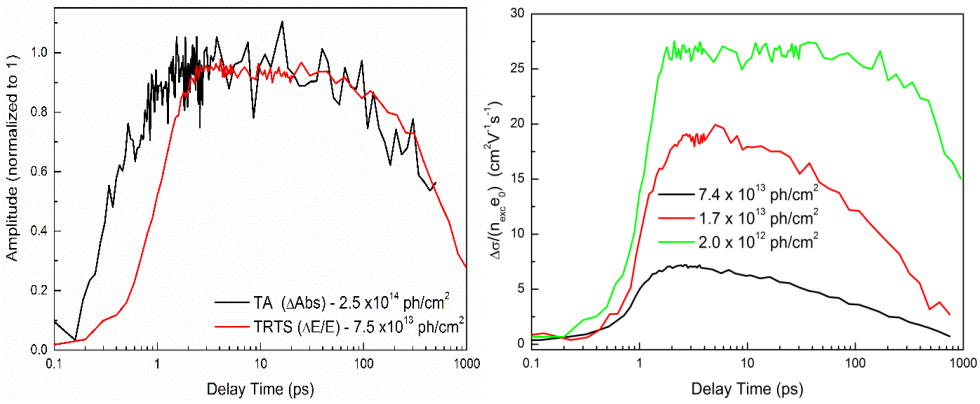

Figure 4. a. Comparison TA and TRTS kinetics for neat $MAPbI_3$ showing similar decay rates up to 1 ns. b. Intensity dependence THz kinetics of $MAPbI_3/Al_2O_3$. (Reprinted with permission from [57], Copyright 2014, American Chemical Society)

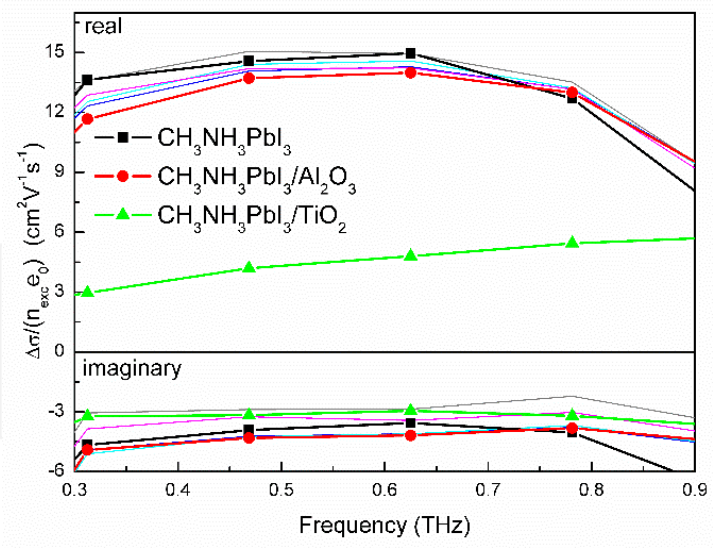

Figure 5. Photoconductivity spectra of $MAPbI_3/Al_2O_3$ at pump-probe delay of 10 ps normalized with $n_{exc}e$ (line with symbols). Solid lines are spectra at 100 ps (blue), 200 ps (cyan), 600 ps (magenta), and 950 ps (gray). (Reprinted with permission from [57], Copyright 2014, American Chemical Society)

Besides the ultrafast generation of highly mobile charges and balanced transport, another very important characteristic required for highly efficient solar cell is the timescale of recombination. It is desirable that charge carriers do not meet since every charge pair that recombines means one charge pair is not extracted. By using the TRMC, the photoconductivity measured by TRTS can be extended from tens of ns to a hundred microseconds. In addition, due to the superior stability of MW emitter, a significant increase in signal-to-noise is achieved allowing the use of excitation density two orders lower than TRTS. As a result, excitation-dependent second-order recombination is minimized, giving more precise dynamical information on recombination of charges. Figure. 6a is the plot of TRMC photoconductivity kinetics of the three samples measured at 5.9×10^9 ph/cm^2 per pulse for 1 μs. For $MAPbI_3$and $9MAPbI_3/Al_2O_3$, the mobility is 3 $cm^2V^{-1}s^{-1}$, while for $MAPbI_3/TiO_2$ it is 1 $cm^2V^{-1}s^{-1}$. The intrinsic mobility of electron in TiO_2 as measured by TRMC has been previously reported as <<0.1 $cm^2V^{-1}s^{-1}$ [18,19]. As ultrafast injection in this material has been discussed above, the 1 $cm^2V^{-1}s^{-1}$ of mobility in $MAPbI_3/TiO_2$ should be coming from holes only. Ergo, the mobility of electrons in $MAPbI_3$ and $MAPbI_3/Al_2O_3$ is 2 $cm^2V^{-1}s^{-1}$, which is consistent with the analysis of TRTS data. Such very high mobility is unique to this material especially in this later timescale since organic solar cell P3HT:PCBM, for example, has 0.045 $cm^2V^{-1}s^{-1}$ only [18]. The signal-to-noise seems worse in Fig. 6a than in Fig. 1b but one should note that there is almost three orders' difference in their excitation intensity. At this very low fluence, the TRMC photoconductivity kinetics of the three materials is rather flat, up to 1 μs. This means that neither the charge population nor the mobility is decaying in this very long timescale. A much longer time window was used to determine the onset of recombination. Figures 6b and 6c are TRMC photoconductivity kinetics of $MAPbI_3/Al_2O_3$ and $MAPbI_3/TiO_2$ obtained from fluences of 5.9×10^9–6×10^{11} ph/cm^2 per pulse, which is 100 times lower than that used in TRTS and at timescale up to 100 μs. The decay is faster at higher intensities and slower with increasing lifetime and amplitude as fluence is lowered, a signature that charges are recombining non-geminately only [20,21]. This also means that there is no first-order recombination even at very low excitation, which suggests charges are diffusing rapidly away from its locus of generation aided by their very high mobility. TRMC signal is similar to photoconductivity measured in TRTS, which means that obtained response is from both charge concentration and mobility. Therefore, a single transient decay trace cannot give information whether it is charge carrier recombination or carrier relaxation that is observed. Nevertheless, it is clear in Fig. 6a that the TRMC kinetics is flat for 1-μs time, which means both its charge population and mobility do not change and any recombination or relaxation of mobility must all be considerably slower than 1 μs. Under ambient sunlight conditions, onset of charge recombination extends to tens of μs, which is the most important conclusion from these results.

Dynamical understanding of charge carriers of the perovskite samples can now be painted from the timescale of sub-ps to a hundred of μs at a wide range of excitation fluences. At excitation densities of 10^{13}-10^{14} ph/cm^2 per pulse (Figs. 1, 2, 4,), second-order non-geminate recombination directly leads to decay of photoconductivity signal. At low excitation fluence, the TRTS kinetics at lowest intensity remained flat up to 1 ns, which means that the carrier

http://dx.doi.org/10.5772/61631

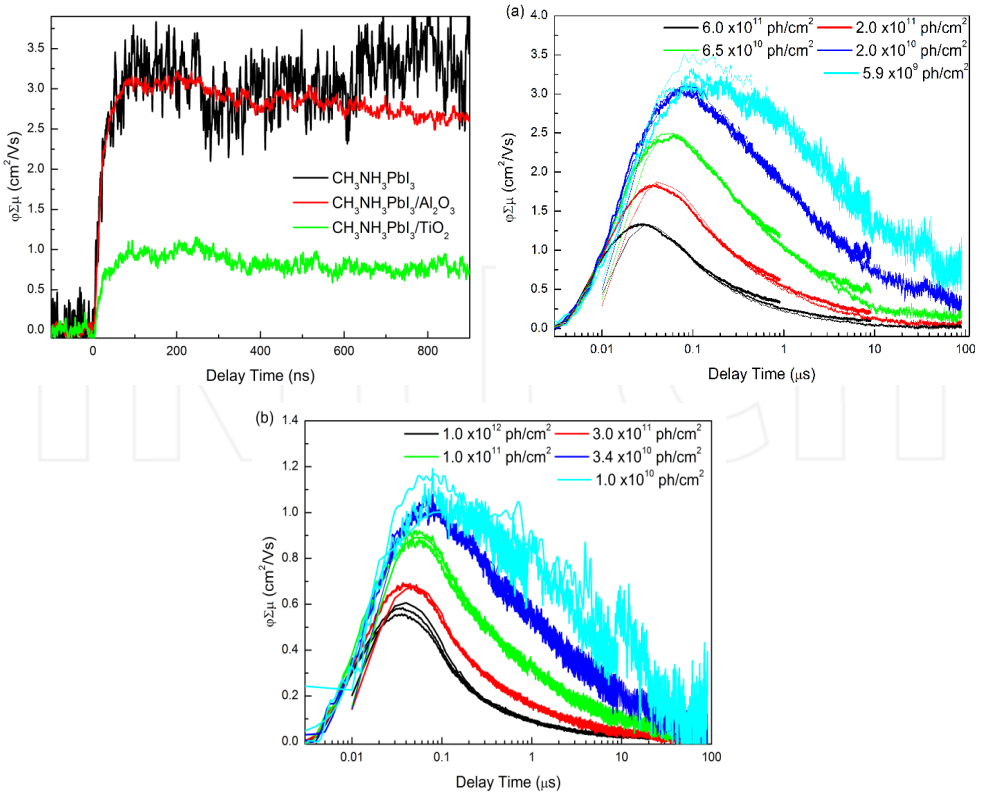

Figure 6. Time-resolved microwave conductivity kinetics of a. $MAPbI_3$, $MAPbI_3/Al_2O_3$, and $MAPbI_3/TiO_2$ measured at 5.9×10^9 ph/cm^2 per pulse for 1 μs and b. at different excitation densities measured up to 100 μs. (Reprinted with permission from [57], Copyright 2014, American Chemical Society)

mobility and its population occurs on a timescale longer than 1 μs, as shown by TRMC traces. Moreover, this means that charges can move over large distances allowing them to be extracted at the electrodes.

As a summary of this section, the combination of several time-resolved spectroscopy techniques, i.e., optical transient absorption, TRTS, and TRMC, characterization of the charge carrier dynamics in neat $MAPbI_3$, and $MAPbI_3$ attached with TiO_2 and Al_2O_3 was presented. Thin film of perovskite and that attached to Al_2O_3 have properties of an ideal solar cell device: Electron and holes are formed in sub-ps timescale with very high mobilities. Its estimated values suggest that they are almost balanced and carriers do not recombine until after tens of microseconds. These characteristics almost guarantee efficient charge collection, a very desirable property of solar cell device. Electron injection to TiO_2 lowers electron mobility resulting to unbalanced charge transport that could lead to built-in electric field. Engineering of electrodes such that balanced transport is still achieved is one possible way of improving its overall power conversion efficiency.

3. Influence of temperature on the charge dynamics

One of the key issues that need to be addressed in studying this class of materials is its dependence on temperature. This is due to the fact that until now there is a disagreement on how the charges are actually generated. As discussed in the previous section, at room temperature the heterogeneity in the exciton binding energy of the material may lead to different rates of charge dissociation. In such case, lowering the temperature should give an indication if it is indeed by excitonic means that charges are created or is it like bulk crystalline silicon that has band-to-band transition. It has been argued that on optical absorption of a photon with energy exceeding the bandgap, an electron is promoted conduction band leaving a hole in the valence band, thereby forming a correlated charge species or exciton. In the presence of, for example, TiO_2 NP electrons into the conduction band is injected thereby freeing exciton. Similar mechanism is found in hole transfer to Spiro-OMeTAD [23-25]. This is in line with the relatively high binding energies (E_B) estimated to be in the range of 19 and 45 meV for $MAPbI_3$ [26,27]. However, by replacing the TiO_2 with insulating Al_2O_3, where no injection is observed (see discussion above) and therefore exciton remained bound, similar high PCE has been achieved by Snaith et al. In fact, it was shown that it works efficiently well in a flat p-i-n configuration, where perovskite active layer serves as both light absorber, charge generation site and transporter [13,28,29]. Moreover, as presented in Section 1, both the TRTS and TRMC obtained very high mobility in the absence of electron or hole transporting electrodes, i.e., for neat $MAPbI_3$ and $MAPbI_3/Al_2O_3$. Due to these results, questions arise on the excitonic characteristics of the initial photoproduct. Crystallographic data show two-phase transitions, orthorhombic to tetragonal at about 160 K and tetragonal to cubic transition at 330 K [30-32]. By using PL and TRMC, exciton dissociation, charge carrier generation, and recombination is explored from 80 K to 300 K to elucidate the role of binding energy in determining the ratio between bound electron hole pairs and mobile charges. PL probes the emission from bound electron hole pairs, while TRMC probes unbound charges.

Shown in Fig. 7 is the plot of the peak emission intensity of $MAPbI_3$ as a function of temperature. A decrease in temperature results in a more intense emission which is a strong indication that generation of charges is thermally activated. At room temperature, the maximum number of mobile charges generated is reached where emission is at minimum. Using equation 1 of Ref. [33], an activation energy (E_B) of 32 ± 5 meV is obtained. It should be noted though that this E_B is specific to this particular sample and could vary depending on the preparation conditions as well as according to the technique used to probe it. In comparison with organic solar cell (E_B=0.3 eV-0.4 eV) [34], the binding energy obtained here is at least ten times lower and very similar to that of silicon, 15 meV. If one assumes that photoexcitation results only in emission or in charge carriers, then the resulting fit in Fig. 7 represents the charge carrier yield as a function of temperature as shown by the black trace.

Figure 8 are plots of TRMC kinetics for $MAPbI_3/Al_2O_3$ normalized with excitation intensity varied over a factor of 50 and measured at 165 K, 240 K, and 300 K. On the one hand, the fastest decay is observed at highest excitation intensity of the traces at 300 K, implying second-order recombination. On the other hand, at low intensities the lifetime of the charge carriers exceeds

http://dx.doi.org/10.5772/61631

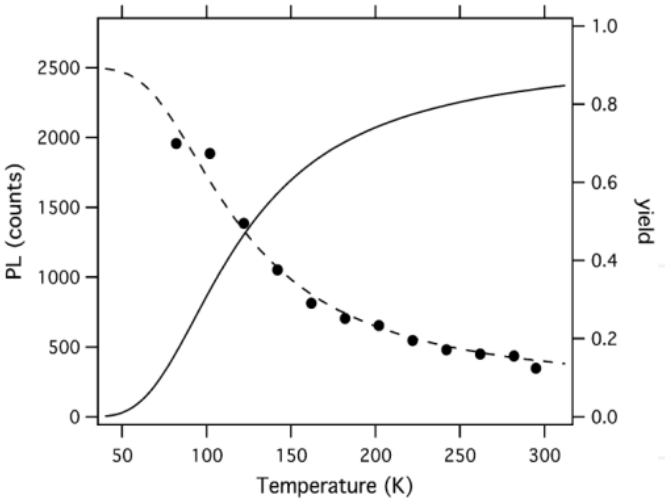

Figure 7. Temperature dependence of PL intensity of $MAPbI_3$ (black circles, λ_{exc} = 550 nm, λ_{dec} = 760 nm). Dashed line is exponential fit, while full line represents the yield of charges on assuming that photoexcitations lead either to radiative decay or to generation of charges. (Reprinted with permission from [33], Copyright 2014, American Chemical Society)

5 μs. Since the decay of TRMC kinetics is a lot slower than corresponding luminescence lifetimes (10 ns) [3,35] at similar intensities, it means that despite the radiative recombination in the ns timescale, there are long-lived charge carriers that survived and remained mobile. More importantly, the mobility of the charges is strongly dependent on the temperature, i.e., from 10.0 $cm^2V^{-1}s^{-1}$ at 165 K to 7.2 $cm^2V^{-1}s^{-1}$ at 240 K and 4.7 $cm^2V^{-1}s^{-1}$ at 300 K. If at these temperatures the changes in the photoconductivity are caused by the change in the yield of charges, then it should have been observed in the PL yield in Fig. 7. Hence, one can assign the changes as due to mobility only. The dependence of mobility on temperature is attributed to quieting of phonon at low temperature with $T^{-1.6}$ dependence, very similar to that of silicon [36]. An increase in mobility usually entails that the second-order recombination would be more efficient since there is higher probability of charges to meet. However, this is not the case in this material. With the increase of mobility, second-order recombination rate diminishes by a factor of 6, which is more than 100 times slower than the reported Langevin recombination, i.e., diffusion controlled recombination [4]. This is a strong indication that there is a barrier in recombination, which should be a temperature-activated process, i.e., meeting of electrons and holes does not necessarily result in recombination. Calculation results yielded a thermal activation over an energy barrier estimated to be ~75 meV [33]. There are two possible origins of this behavior currently reported in the literature: (1) due to the induced dipole moment brought about by the intermittent rotation of MA ions [30,37] and the (2) preferential spatial localization of charge carriers in different parts/materials of the perovskite unit cell. Density functional theory calculations have revealed that 6s- and 5p-orbitals of lead and iodine, respectively, consist of the maxima of the valence band, while 6p-orbitals of lead is where conduction band minima is mostly incorporated [38].

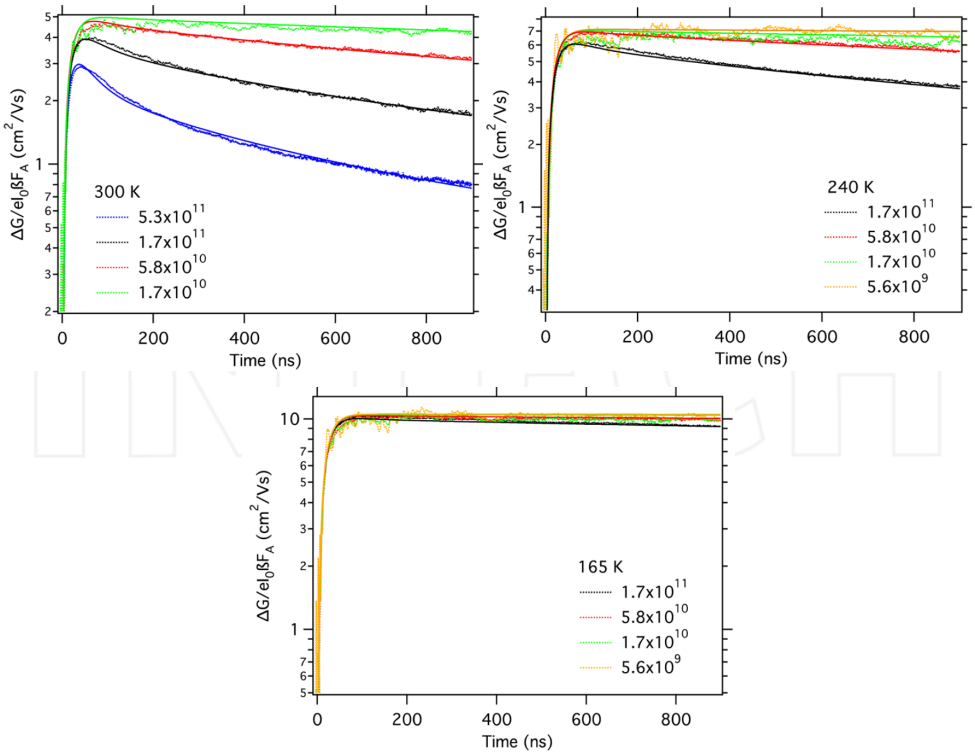

Figure 8. TRMC kinetics of $MAPbI_3/Al_2O_3$ at several excitation intensities measured at 165 K, 240 K, and 300 K (λ_{exc} = 410 nm). (Reprinted with permission from [33], Copyright 2014, American Chemical Society)

Temperature dependent behavior of MAPbI3 is presented in this section. Results show that this material has very similar characteristics as silicon, i.e. it has low exciton binding energy (32 meV)and its mobility has $T^{-1.6}$ dependence brought about by quieting of phonons. More importantly, charges carrier do not recombine when it they meet but instead require a thermal activation over an energy barrier of 75 meV, allowing the charges to be collected at the electrodes efficiently.

4. Role of dark carriers

In this section, the intrinsic property of $MAPbI_3$ is examined when organic electrodes, PCBM and Spiro-OMeTAD are deposited on top of the neat perovskite material. From these samples, the timescale of injection of charges and the dynamics of its recombination are analyzed. Plotted in Fig. 9 are the TRTS kinetics of neat $MAPbI_3$, $MAPbI_3$/PCBM, and $MAPbI_3$/Spiro-OMeTAD normalized with excitation density. At the earliest timescale, the mobility is found to be ~15 $cm^2V^{-1}s^{-1}$ for this particular neat $MAPbI_3$ sample. This mobility slightly decreased

http://dx.doi.org/10.5772/61631

after 1 ns due to second-order recombination, similar to that shown in Fig. 4b. In contrast, the decay of $MAPbI_3$/PCBM is faster, down to almost a third at the same timescale and initial mobility. Such decay is more clearly seen at 7 ns time window in Fig. 9b. For $MAPbI_3$/Spiro-OMeTAD, the initial mobility is 5 $cm^2V^{-1}s^{-1}$, i.e., three times smaller than the neat but remains flat up to 1 ns. At the later timescale, i.e., hundreds of ns to us (Fig. 10a), rapid decay is still seen in $MAPbI_3$/PCBM, while neat $MAPbI_3$ and $MAPbI_3$/Spiro-OMeTAD have very similar, if not identical, slower decay. In Fig.10b, the TRMC kinetics is normalized with excitation density and the corresponding mobility is plotted versus incident photon flux. For the neat $MAPbI_3$, mobility decreases on increasing fluences (>10^{11} ph/cm^2) due to second-order recombination. This behavior is also seen in the bilayer samples, but for $MAPbI_3$/PCBM, the threshold for this process is shifted to higher fluence (>10^{12} ph/cm^2).

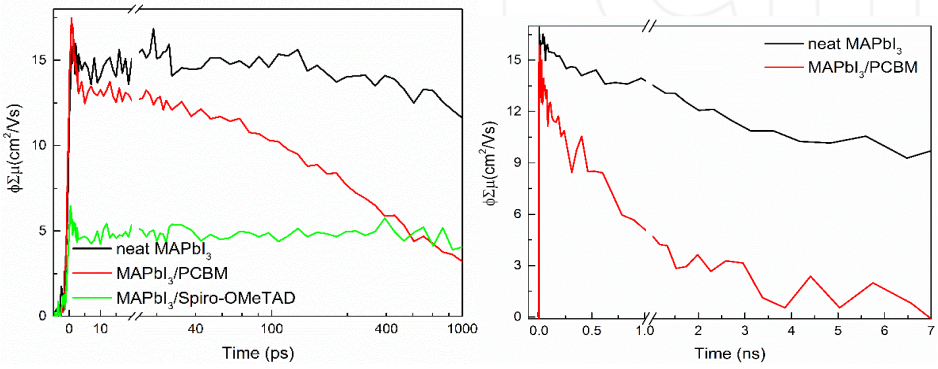

Figure 9. a. TRTS kinetics of neat $MAPbI_3$, $MAPbI_3$/PCBM, and $MAPbI_3$/Spiro-OMeTAD normalized to the excitation intensity (λ_{pump} = 590 nm). b. TRTS kinetics with 7 ns time window.

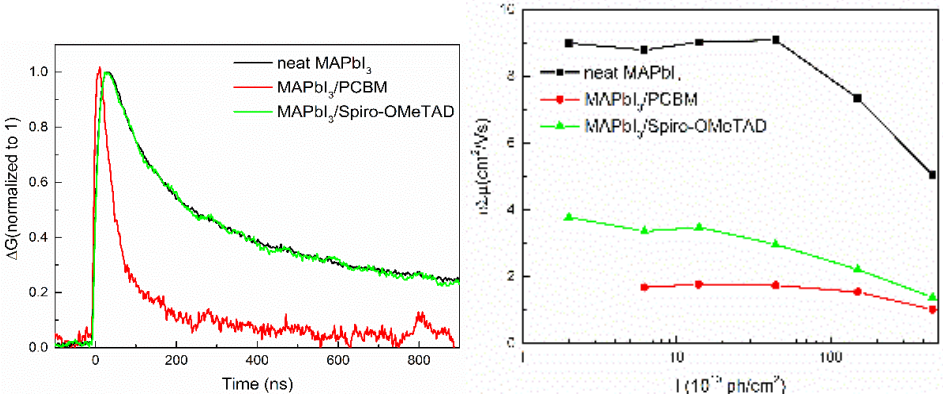

Figure 10. a. TRMC traces for the three samples recorded at an excitation intensity of 1.0 × 10^{11} photons/cm^2 per pulse (λ_{pump} = 600 nm) and normalized to unity. b. Mobility versus incident intensity for neat $MAPbI_3$ and bilayers.

It has been shown that Spiro-OMeTAD is a good hole transporting material (HTM) as it has been extensively used in solar cell devices. One of its favorable characteristics is its 0.5 eV valence band offset with respect to $MAPbI_3$ [23,39,40,41]. However, in order to extract decent PCE, additives like lithium bis(trifluoromethanesulfonyl) imide (LiTFSI) are necessary, which enables this HTM to substantially increase its very low intrinsic hole mobility, i.e., 10^{-8} S/cm [25,42]. Using TRTS, the mobility of $MAPbI_3$/Spiro-OMeTAD is found to be three times lower (5 $cm^2V^{-1}s^{-1}$) than in neat $MAPbI_3$ (15 $cm^2V^{-1}s^{-1}$) (see Fig. 9a). In agreement with this measurement, the mobility measured by TRMC has similar decrease, i.e., from 9 $cm^2V^{-1}s^{-1}$ in neat $MAPbI_3$ to 3.5 $cm^2V^{-1}s^{-1}$ in $MAPbI_3$/Spiro-OMeTAD (Fig. 10b). The decrease in the mobility can be interpreted as disappearance of either electrons or holes in the neat $MAPbI_3$ as a result of charge transfer. On the basis that Spiro-OMeTAD is an HTM, it should therefore be the holes that disappeared and were injected. The hole transfer is confirmed by both techniques and the timescale of injection as seen by TRTS is sub-ps. This suggests that the energy offset at the interface alone is sufficient to allow efficient sub-ps hole injection despite the fact that in this sample no additive was added. This finding consequently means that the mobility of 5 $cm^2V^{-1}s^{-1}$ in TRTS and 3.5 $cm^2V^{-1}s^{-1}$ in TRMC should have originated from electrons that are left in $MAPbI_3$. This process is schematically shown in Figure 11. From the initial 15 $cm^2V^{-1}s^{-1}$ in neat $MAPbI_3$ and 5 $cm^2V^{-1}s^{-1}$ in $MAPbI_3$/Spiro-OMeTAD (both from TRTS), this leads to a hole mobility of 10 $cm^2V^{-1}s^{-1}$ in the perovskite, implying that holes should have diffused at least 30 nm within 1 ps, which is consistent with a sub-ps injection time. Piatkowski et al. also recently reported that timescale of hole injection is 0.7 ps as measured by transient absorption spectroscopy [43].

It has been reported that that charge transfer over an interface typically leads to different decay kinetics as compared to dynamics of the carriers generated in a single semiconductor [44]. However, in the case of $MAPbI_3$/Spiro-OMeTAD, although hole injection is confirmed by TRTS, its decay in TRMC is similar to the neat $MAPbI_3$. In fact, even at different excitation intensity their decay is still very similar as shown in Fig. 12a. The identical TRMC kinetics imply that their decay pathways must be identical, if not very similar. It was previously reported that depending on the preparation conditions, perovskite could either be an n-doped or a p-doped semiconductor. For example, in the work of Leijtens et al., an n-type perovskite material was obtained when deposited to Al_2O_3 NPs [45]. In contrast, calculation of Shi et al. [46] suggests that p-type is usually obtained; while Kim et al. [47] reported that it can be controlled as n- or p-type depending on the defects. It is therefore not unrealistic, at least for a moment, to postulate that perovskite measured here has concentration of holes already in the dark (p_0), i.e., that $MAPbI_3$ is an unintentionally doped, p-type semiconductor. This would mean that once carriers are photogenerated and holes transferred to Spiro-OMeTAD, electrons left in the conduction band of $MAPbI_3$ will recombine with both, the dark holes in the valence band of $MAPbI_3$ and the photogenerated holes injected into Spiro-OMeTAD. So long as the concentration of photogenerated electrons is smaller than the total concentration of holes (dark and light-induced carriers), the electron hole recombination kinetics in $MAPbI_3$ should be barely dependent on whether there is hole injection or not. This scenario would then result in conductivity decay very similar to neat $MAPbI_3$. Since the obtained kinetics are identical, it can be surmised that the perovskite sample measured here is p-type. It should also be stressed

http://dx.doi.org/10.5772/61631

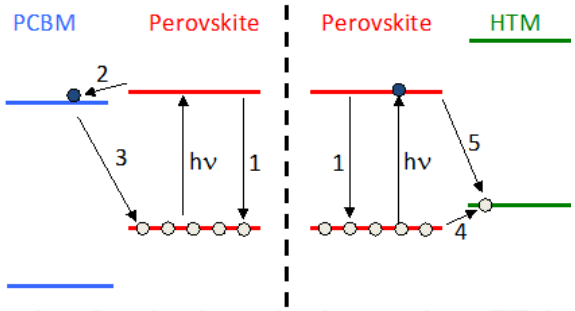

Figure 11. Schematic diagram of injection and recombination dynamics in from neat $MAPbI_3$ to PCBM and Spiro-OMeTAD.

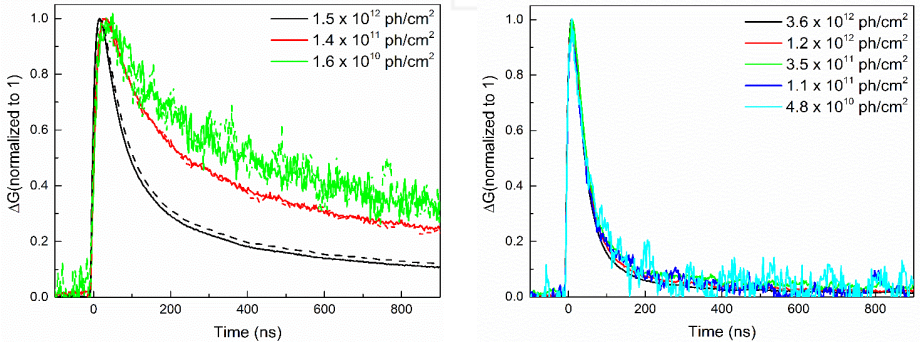

Figure 12. Excitation intensity dependence of TRMC kinetics of (a) $MAPbI_3$/Spiro-OMeTAD and (b) $MAPbI_3$/PCBM.

that both TRTS and TRMC probe only the change in conductivity due to optical excitation but not the dark conductivity.

For electron acceptors, PCBM has been extensively used for organic solar cells and lately has been also utilized for perovskite-based solar cells as well. Despite its small energy offset with respect to perovskite, the reported power conversion efficiency is over 10% [48,49]. This indicates that electrons are transferred from the perovskite to PCBM, which is schematically represented as process 2 in Fig. 11. The electron mobility in PCBM is quite small, i.e., 10^{-3} $cm^2V^{-1}s^{-1}$ [49-53], and therefore contributing insignificantly to the measured mobility in both TRTS and TRMC. Hence, the measured signal in Figs. 9 and 10b, only represent the mobile photogenerated charges in the perovskite. This implies that the decay measured in photoconductivity kinetics could represent not only charge recombination within the $MAPbI_3$ (process 1), electron injection from $MAPbI_3$ to PCBM (process 2), but the recombination at $MAPbI_3$/PCBM interface (process 3) as well. To disentangle the contributions of these processes, one can consider this qualitative consideration: that electron injection (process 2) is much faster than interfacial recombination between holes left in the perovskite and electrons injected to

PCBM (process 3). In this scenario, a clear nonexponential, slower decay is expected since mobile electrons in $MAPbI_3$ become immobile in PCBM. However, since there is no such plateau observed (Fig. 9b), it can be concluded that the rate constant for the interfacial electron hole recombination (process 3) is similar to, or exceeds, the electron injection rate, which is consistent with the fact that the difference in the energy gap in their conduction bands is small.

At the earliest timescale of the THz kinetics, $MAPbI_3$/PCBM bilayer and neat $MAPbI_3$ have the same mobility (~15 $cm^2V^{-1}s^{-1}$; Figs. 9a and 9b). This shows that mobile charges are rapidly formed (<1 ps) and that the photogenerated charges stay in the perovskite for at least a few ps. After 1 ns, the mobility is reduced to approximately a third, suggesting that charges disappear on this timescale. As discussed above, there are three different processes either consecutively or simultaneously occurring that may be responsible for this decay. The very small energy offset at the interface between $MAPbI_3$ and PCBM could retard electron injection to the ns timescale. Transient absorption spectroscopy as reported by Xing et al. estimated electron injection from perovskite to PCBM to be within several ns [17]. Therefore, electron injection into PCBM can be one of the processes leading to the THz decay. The second plausible origin of the THz decay is the inevitable recombination of electrons injected in the PCBM, which are pinned at the interface due to their low mobility, with dark and photogenerated holes in perovskite. Similar to $MAPbI_3$/Spiro-OMeTAD, concentration of dark holes here is expected to be at least the same order since the preparation method used is similar. Third, the excitation-dependent second-order recombination within the perovskite process could also manifest as decay of the conductivity signal. The THz kinetics of neat $MAPbI_3$ (Figs. 9 a and Figs. 9) show that at 2.1×10^{12} ph/cm^2 per pulse, this process occurs on the many ns timescale, significantly slower than the decay of the $MAPbI_3$/PCBM conductivity. Hence, this process only weakly contributes. The THz conductivity decay can therefore be assigned to convolution of electron injection to PCBM and electron–hole recombination at the perovskite/PCBM interface wherein both processes are occurring on a similar timescale.

The TRMC measurements of $MAPbI_3$/PCBM in Fig. 10a show extended time window of conductivity measurements and were obtained at lower excitation intensity than the TRTS measurements. Because of this, the second-order recombination could only occur on the microsecond timescale [33] and will only marginally influence the decay. Hence, the origin of the decay should only be from electron injection and interfacial recombination. The excitation-dependent mobility in Fig. 10b provides another indication of the timescale of electron injection and interfacial recombination. On the one hand, $MAPbI_3$/PCBM has mobility of 2 $cm^2V^{-1}s^{-1}$, representing mobile holes only since injection is apparent. On the other hand, $MAPbI_3$/Spiro-OMeTAD has hole mobility of 5.5 $cm^2V^{-1}s^{-1}$, i.e., 9 $cm^2V^{-1}s^{-1}$ from the neat minus 3.5 $cm^2V^{-1}s^{-1}$. There is almost a three-time difference between the hole mobilities measured from the two samples. Assuming 100% electron injection into PCBM after several ns, it means that two-thirds of the photogenerated mobile holes have disappeared, most probably through interfacial recombination, on the timescale similar to injection time. Admittedly, Wojciechowski et al. reported TRMC kinetics decay similar to that observed here. However, the decay was assigned to electron injection under the assumption that the difference electron and hole mobility is at least ten times [54]. This is in contrast with several theoretical papers on the electrons and holes'

http://dx.doi.org/10.5772/61631

effective masses stating that they do not differ more than a factor 2 [16,55,56], to experimental works showing balanced electron–hole diffusion lengths [3,17], and to previous THz and TRMC conductivity measurements [33,57]. Moreover, using the results presented here it is possible to understand the TRMC kinetics as ns electron injection into PCBM in convolution with interfacial recombination between immobile electrons in PCBM and photogenerated and dark holes in the perovskite. The resulting picture is an oppositely charged bilayer material wherein recombination dynamics is not influenced by the excitation density. In fact, as shown in Figure 12b, the TRMC kinetic decays of $MAPbI_3$/PCBM do not have any dependency on excitation. This is a strong indication of the first-order character of the recombination.

These results have far-reaching implications in understanding the fundamental photophysical processes in these materials and to the operation of perovskite solar cells. Utmost care should be taken in interpreting photophysical data as these are strongly influenced by the state and population of defects that control their doping, as reported by several papers [45-47]. Recombination at the $MAPbI_3$/PCBM interface represents a loss mechanism and therefore is detrimental in the operation of solar cells. Similar to strategy in optimizing the performance of perovskite devices by adding dopants to Spiro-OMeTAD in order to increase its conductivity, PCBM should also be doped. Moreover, developing new methods in reducing unintentional doping would certainly be beneficial. In summary of this section, it was found that hole transfer from $MAPbI_3$ into Spiro-OMeTAD occurs on a sub-ps timescale, while its recombination dynamics is identical to neat $MAPbI_3$ and controlled by a high concentration of dark holes. Electron injection in PCBM is slower, few ns, which is convoluted with the interfacial recombination between the electrons residing in PCBM and the photogenerated and dark holes in $MAPbI_3$. The positively charged majority carriers brought about by unintentional doping, dictate not only the recombination of photoexcited carriers in neat $MAPbI_3$ layer but also control the charge injection dynamics in bilayer samples. Finally, reduction of the hole concentration in the perovskite could help to retard the recombination yielding a higher overall power conversion efficiency.

5. Conclusion

Despite the advancement in the understanding of the device properties of perovskite solar cells, research on its fundamental electrical characteristics have remained scarce. This work has shown that using time-resolved THz spectroscopy and microwave conductivity measurements, complemented by transient absorption and photoluminescence spectroscopy, an in-depth understanding may be achieved. Among its nearly ideal solar cell characteristics are ultrafast charge generation (<0.2 ps), high mobility (μ_e = 12.5 $cm^2V^{-1}s^{-1}$ and μ_h = 7.5 $cm^2V^{-1}s^{-1}$) which remained constant up to at least 1 ns, charge lifetime of tens of μs, and recombination barrier energy of 75 meV. One of the challenges that need to be addressed by the solar cell community is to standardized protocol on growth/preparation methods such that the state and concentration of defects, thereby, dark carriers will be controlled as desired. As presented in this chapter, such dark carriers play a vital role in recombination dynamics and hence could spell success or failure of the device.

Acknowledgements

This work was supported by the Swedish Energy Agency (STEM), the Swedish Research Council, the Knut&Alice Wallenberg Foundation, the European Research Council (Advanced Investigator Grant to VS, 226136-VISCHEM), the Nanometer Consortium at Lund University (nmc@LU), and the Lund Laser Center. The time-resolved THz setup is partly developed by Pascher Instruments (www.pascherinstruments.com). The author would also like to express his gratitude to Prof. Tom J. Savenije of Delft University of Technology, The Netherlands, where all the TRMC measurements were done. Finally, this work is dedicated to Prof. Villy Sundström, a mentor, a colleague, and a friend.

Author details

Carlito S. Ponseca Jr.*

Address all correspondence to: carlito.ponseca@chemphys.lu.se

Division of Chemical Physics, Lund University, Lund, Sweden

References

[1] Kojima A, Teshima K, Shirai Y, Miyasaka T. Organometal Halide Perovskites as Visible-Light Sensitizers for Photovoltaic Cells. *J Am Chem Soc* 2009; 48: 6050–6051.

[2] Anon National Renewable Energy Labs (NREL) efficiency chart (2015); http://www.nrel.gov/ncpv/images/efficiency_chart.jpg Natl Renew Energy Labs Effic chart (2015); http//www.nrel.gov/ncpv/images/efficiency_chart.jpg

[3] Stranks SD, Eperon GE, Grancini G, et al. Electron-Hole Diffusion Lengths Exceeding 1 micrometer in an Organometal Trihalide Perovskite Absorber. *Science* 2013; 342:341–344.

[4] Wehrenfennig C, Eperon GE, Johnston MB, et al. High Charge Carrier Mobilities and Lifetimes in Organolead Trihalide Perovskites *Adv Mater* 2013; 26:1584–1589.

[5] Ponseca CS, Yartsev A, Wang E, Andersson MR, et al. Ultrafast Terahertz Photoconductivity of Bulk Heterojunction Materials Reveals High Carrier Mobility up to Nanosecond Time Scale. *J Am Chem Soc* 2012; 134:11836–11839.

[6] Ponseca CS, Němec H, Vukmirović N, et al. Electron and Hole Contributions to the Terahertz Photoconductivity of a Conjugated Polymer:Fullerene Blend Identified *J Phys Chem Lett* 2012; 3:2442–2446.

[7] Nemec H, Rochford J, Taratula O, et al. Influence of the Electron-Cation Interaction on Electron Mobility in Dye-Sensitized ZnO and TiO_2 Nanocrystals: A Study Using Ultrafast Terahertz Spectroscopy. *Phy Rev Lett* 2010; 104:197401.

[8] Žídek K, Zheng K, Ponseca CS, et al. Electron Transfer in Quantum-Dot-Sensitized ZnO Nanowires: Ultrafast Time-Resolved Absorption and Terahertz Study. *J Am Chem Soc* 2012; 134:12110–12117.

[9] Ponseca CS, Nemec H, Wallentin J, et al. Bulk-Like Transverse Electron Mobility in an Array of Heavily n-Doped InP Nanowires Probed by Terahertz Spectroscopy. *Phys Rev B* 2014; 90:085405.

[10] Rothenberger G, Fitzmaurice D, Gratzel M. *J Phys Chem* 1992; 96:5983-5987.

[11] Lin Q, Armin A, Nagiri RR, Burn PL, et al. Electro-Optics of Perovskite Solar Cells. *Nat Photonics* 2014; 9:106–112.

[12] Sum TCT, Mathews N. Advancements in Perovskite Solar cells: Photophysics behind the Photovoltaics. *Energy Environ Sci* 2014; 7:2518–2534.

[13] Lee MM, Teuscher J, Miyasaka T., et al. Efficient Hybrid Solar Cells Based on Meso-Superstructured Organometal Halide Perovskites. *Science* 2012; 338:643–645.

[14] Blom PWM, Mihailetchi VD, Koster LJA, et al. Device Physics of Polymer:Fullerene Bulk Heterojunction Solar Cells. *Adv Mater* 2007; 19:1551–1556.

[15] Hendry E, Koeberg M, O'Regan B. Local Field Effects on Electron Transport in Nano-structured TiO2 Revealed by Terahertz Spectroscopy. *Nano Lett* 2006; 6:755–759.

[16] Quarti C, Mosconi E, De Angelis F. Interplay of Orientational Order and Electronic Structure in Methylammonium Lead Iodide: Implications for Solar Cell Operation. *Chem Mater* 2014; 26:6557–6569.

[17] Xing G, Mathews N, Sun S, et al. Long-Range Balanced Electron- and Hole-Transport Lengths in Organic-Inorganic CH3NH3PbI3. *Science* 2013; 342:344–347.

[18] Murthy DHK, Gao K, Vermeulen MJW, et al. Mechanism of Mobile Charge Carrier Generation in Blends of Conjugated Polymers and Fullerenes: Significance of Charge Delocalization and Excess Free Energy. *J Phys Chem C* 2012; 116:9214–9220.

[19] Fravventura, MC, Deligiannis D, Schins JM, et al. What Limits Photoconductance in Anatase TiO2 Nanostructures? A Real and Imaginary Microwave Conductance Study. *J Phys Chem C* 2013; 117:8032–8040.

[20] De S, Pascher T, Maiti M, et al. Geminate Charge Recombination in Alternating Polyfluorene Copolymer/Fullerene Blends. *J Am Chem Soc* 2007; 129:8466–8472.

[21] Pal SK, Kesti T, Maiti M, et al. Geminate Charge Recombination in Polymer/Fullerene Bulk Heterojunction Films and Implications for Solar Cell Function. *J Am Chem Soc* 2010; 132:12440–12451.

[22] Bi D, Yang L, Boschloo G, et al. Effect of Different Hole Transport Materials on Recombination in CH3NH3PbI3 Perovskite-Sensitized Mesoscopic Solar Cells. *J Phys Chem Lett* 2013; 4:1532−1536.

[23] Kim HS, Lee C-R, Im J.H, et al. Lead Iodide Perovskite Sensitized All-Solid-State Submicron Thin Film Mesoscopic Solar Cell with Efficiency Exceeding 9%. *Sci Rep* 2012; 2:591-595.

[24] Jeng, JY, Chiang, YF, Lee MH, et al. CH3NH3PbI3 Perovskite/Fullerene Planar- Heterojunction Hybrid Solar Cells. *Adv Mater* 2013; 25:3727−3732.

[25] Marchioro A, Teuscher J, Friedrich D, et al. Unravelling the Mechanism of Photoinduced Charge Transfer Processes in Lead Iodide Perovskite Solar Cells. *Nat Photonics* 2014; 8:250−255.

[26] Ishihara T. Optical-Properties of PbI-Based Perovskite Structures. *J Lumin* 1994; 60(1): 269−274.

[27] Sun S, Salim T, Mathews N, et al. The Origin of High Efficiency in Low-Temperature Solution-Processable Bilayer Organometal Halide Hybrid Solar Cells. *Energy Environ Sci* 2014; 7:399−407.

[28] Liu M, Johnston MB, Snaith HJ. Efficient Planar Heterojunction Perovskite Solar Cells by Vapour Deposition. *Nature* 2013; 6:1739−1743.

[29] Ball JM, Lee MM, Hey A, Snaith HJ. Low-Temperature Processed Meso-Superstructured to Thin-Film Perovskite Solar Cells. *Energy Environ Sci* 2013; 6:1739−1743.

[30] Wasylishen RE, Knop O, Macdonald JB. Cation Rotation in Methylammonium Lead Halides. *Solid State Commun* 1985; 56:581−582.

[31] Onodayamamuro N, Yamamuro O, Matsuo T, Suga HP-T. Phase-Relations of CH3NH3PbX3 (X = CL, BR, I) Crystals. *J Phys Chem Solids* 1992; 53:277−281.

[32] Onodayamamuro N, Matsuo T, Suga H. Dielectric Study of CH3NH3PbX3 (X = CL, BR, I). *J Phys Chem Solids* 1992; 53:935−939.

[33] Savenije TJ, Ponseca CS, Kunneman L, et al. Thermally Activated Exciton Dissociation and Recombination Control the Carrier Dynamics in Organometal Halide Perovskite *J Phys Chem Lett* 2014; 5:2189−94.

[34] Servaites JD, Ratner MA, Marks TJ. Organic Solar Cells: A New Look at Traditional Models. *Energy Environ Sci* 2011; 4:4410−4422.

[35] Stoumpos CC, Malliakas, CD, Kanatzidis MG. Semiconducting Tin and Lead Iodide Perovskites with Organic Cations: Phase Transitions, High Mobilities, and Near-Infrared Photoluminescent Properties. *Inorg Chem* 2013; 52:9019−9038.

[36] van Zeghbroeck B. Principles of Semiconductor Devices. University of Colorado: Boulder CO, 2006.

[37] Knop O, Wasylishen RE, White MA, et al. Alkylammonium Lead Halides 0.2. CH3NH3PbCl3, CH3NH3PbBr3, CH3NH3PbI3 Perovskites – Cuboctahedral Halide Cages with Isotropic Cation Reorientation. *Can J Chem: Rev Can Chim* 1990; 68:412–422.

[38] Even J, Pedesseau L, Jancu JM, Katan C. Importance of Spin–Orbit Coupling in Hybrid Organic/Inorganic Perovskites for Photovoltaic Applications. *J Phys Chem Lett* 2013; 4:2999–3005.

[39] Abrusci A Stranks SD, Docampo P, et al. High-Performance Perovskite-Polymer Hybrid Solar Cells via Electronic Coupling with Fullerene Monolayers. *Nano Lett* 2013; 13:3124–3128.

[40] Shen Q, Ogomi Y, Chang J, et al. Charge Transfer and Recombination at the Metal Oxide/CH3NH3PbClI2/spiro-OMeTAD Interfaces: Uncovering the Detailed Mechanism behind High Efficiency Solar Cells. *Phys Chem Chem Phys* 2014; 16:19984–19992.

[41] Edri E, Kirmayer S, Mukhopadhyay S, et al. Elucidating the Charge Carrier Separation and Working Mechanism of CH3NH3PbI3−xClx Perovskite Solar Cells. *Nat Commun* 2014; 5:3461–3465.

[42] Nguyen WH, Bailie, CD, Unger EL, McGehee MD. Enhancing the Hole-Conductivity of Spiro-OMeTAD without Oxygen or Lithium Salts by Using Spiro (TFSI) 2 in Perovskite and Dye-Sensitized Solar Cells. *J Am Chem Soc* 2014; 36:10996–11001.

[43] Piatkowski P, Cohen B, Javier Ramos F, et al. Direct Monitoring of Ultrafast Electron and Hole Dynamics in Perovskite Solar Cells. *Phys Chem Chem Phys* 2015; 17:14674–14684.

[44] Kroeze JE, Savenije TJ, Vermeulen MJW, Warman JM. Contactless Determination of the Photoconductivity Action Spectrum, Exciton Diffusion Length, and Charge Separation Efficiency in Polythiophene-Sensitized TiO2 Bilayer. *J Phys Chem B* 2003; 107:7696–7705.

[45] Leijtens T, Stranks SD, Eperon GE, et al. Electronic Properties of Meso-Superstructured and Planar Organometal Halide Perovskite Films: Charge Trapping, Photodoping, and Carrier Mobility. ACS Nano 2014; 8:7147–7155.

[46] Shi T, Yin W-J, Yan Y. Predictions for p-Type CH3NH3PbI3 Perovskites. *J Phys Chem C* 2014; 118:25350–25354.

[47] Kim J, Lee S-H, Lee J-H, Hong K-H. The Role of Intrinsic Defects in Methylammonium Lead Iodide Perovskite. *J Phys Chem Lett* 2014; 5:1312–1317.

[48] Malinkiewicz O, Yella A, Lee YH, et al. Perovskite Solar Cells Employing Organic Charge-Transport Layers. *Nat Photon* 2013; 8:128–132.

[49] Gao P, Grätzel M, Nazeeruddin MK, Organohalide Lead Perovskites for Photovoltaic Applications. *Energy Environ Sci* 2014; 7:2448–2463.

[50] Von Hauff E, Dyakonov V, Parisi J. Study of Field Effect Mobility in PCBM Films and P3HT:PCBM Blends. *Sol Energy Mater Sol Cells* 2005; 87:149–156.

[51] Mihailetchi VD, Xie H, De Boer B, et al. Charge Transport and Photocurrent Generation in Poly(3-hexylthiophene): Methanofullerene Bulk-Heterojunction Solar Cells. *Adv Funct Mater* 2006; 16:699–708.

[52] Warman JM, De Haas MP, Anthopoulos TD, De Leeuw DM. The Negative Effect of High-Temperature Annealing on Charge-Carrier Lifetimes in Microcrystalline PCBM. *Adv Mater* 2006; 18;2294–2298.

[53] Savenije TJ, Ferguson AJ, Kopidakis N, Rumbles G. Revealing the Dynamics of Charge Carriers in Polymer:Fullerene Blends Using Photoinduced Time-Resolved Microwave Conductivity. *J Phys Chem C* 2013; 117:24085–24103.

[54] Wojciechowski K, Stranks, SD, Abate A, et al. Heterojunction Modification for Highly Efficient Organic–Inorganic Perovskite Solar Cells. *ACS Nano* 2014; 8:12701–12709.

[55] Chang Y, Park C, Matsuishi K. First-Principles Study of the Structural and the Electronic Properties of the Lead-Halide-Based Inorganic-Organic Perovskites (CH3NH3)PbX3 and CsPbX3 (X = Cl, Br, I). *J Korean Phys Soc* 2004; 44: 889–893.

[56] Giorgi G, Fujisawa, JI, Segawa H, Yamashita K. Small Photocarrier Effective Masses Featuring Ambipolar Transport in Methylammonium Lead Iodide Perovskite: A Density Functional Analysis. *J Phys Chem Lett* 2013; 4:4213–4216.

[57] Ponseca, CS, Savenije, TJ, Abdellah M, et al. Organometal Halide Perovskite Solar Cell Materials Rationalized: Ultrafast Charge Generation, High and Microsecond-Long Balanced Mobilities, and Slow Recombination. J Am Chem Soc 2014; 136:5189–5192.